Turning Erythrocytes into Functional Micromotors
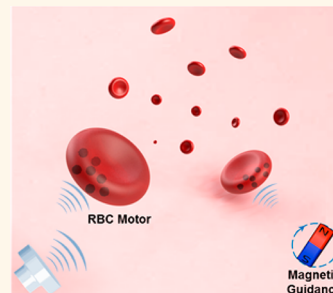
Zhiguang Wu,[†,‡,§] Tianlong Li,[†,§] Jinxing Li,[†,§] Wei Gao,[†] Tailin Xu,[†] Caleb Christianson,[†] Weiwei Gao,[†] Michael Galarnyk,[†] Qiang He,[‡] Liangfang Zhang,*,[†] and Joseph Wang*,[†]

[†]Department of Nanoengineering, University of California, San Diego, La Jolla, California 92093, United States and [‡]The Academy of Fundamental and Interdisciplinary Sciences, Harbin Institute of Technology, Harbin 150080, China. [§]Z.W., T.L., and J.L. contributed equally to this work.

ABSTRACT Attempts to apply artificial nano/micromotors for diverse biomedical applications have inspired a variety of strategies for designing motors with diverse propulsion mechanisms and functions. However, existing artificial motors are made exclusively of synthetic materials, which are subject to serious immune attack and clearance upon entering the bloodstream. Herein we report an elegant approach that turns natural red blood cells (RBCs) into functional micromotors with the aid of ultrasound propulsion and magnetic guidance. Iron oxide nanoparticles are loaded into the RBCs, where their asymmetric distribution within the cells results in a net magnetization, thus enabling magnetic alignment and guidance under acoustic propulsion. The RBC motors display efficient guided and prolonged propulsion in various biological fluids, including undiluted whole blood. The stability and functionality of the RBC motors, as well as the tolerability of regular RBCs to the ultrasound operation, are carefully examined. Since the RBC motors preserve the biological and structural features of regular RBCs, these motors possess a wide range of antigenic, transport, and mechanical properties that common synthetic motors cannot achieve and thus hold considerable promise for a number of practical biomedical uses.

KEYWORDS: synthetic motor · red blood cells · magnetic guidance · ultrasound · whole blood · biocompatibility

The development of nano/micromotors is a research area of intense activity due to numerous potential applications.[1−8] While considerable attention has been given to catalytic motors that exhibit self-propulsion in the presence of a hydrogen peroxide fuel, many practical applications would require elimination of the need of chemical fuel.[9−15] Several groups have thus explored fuel-free propulsion mechanisms based on externally applied magnetic or ultrasound fields.[16−20] The increased capabilities and sophistication of these tiny fuel-free motors hold considerable promise for directed drug delivery, biopsy, cleaning clogged arteries, precision nanosurgery, or localized diagnosis in hard-to-reach places. To fulfill these exciting potential applications, particular attention is drawn to the biocompatibility of the motors in biological environments and to their performance in undiluted biological media. The metallic or polymeric components of common artificial nano/micromotors are facing destructive immune attack once entering into the bloodstream due to the foreign nature of these materials.

Natural cells and their derivatives are highly optimized by nature for their unique *in vivo* functions and possess attractive features desired for systemic cargo delivery.[21−23] As a result, various types of cells, such as red blood cells (RBCs, also named erythrocytes), white blood cells, macrophages, engineered stem cells, and so on, have been employed to carry and deliver therapeutic or imaging agents.[24,25] The intrinsic properties of these natural carriers have opened the door to creative cargo delivery strategies and novel biomaterials development. Among these cell-based carriers, RBCs are of particular interest owing to their vast availability, unique mechanical attribute, surface immunosuppressive property, and versatile cargo-carrying capability.[26−28] As such, numerous RBCs based or inspired delivery systems have been recently developed for cargo delivery, relying on the prolonged transport property of RBCs in the bloodstream.[29−32] However, there are no early reports on how to bestow an active propulsion force upon the passively moving RBCs and thus to utilize the cells as a powerful autonomous micromotor.
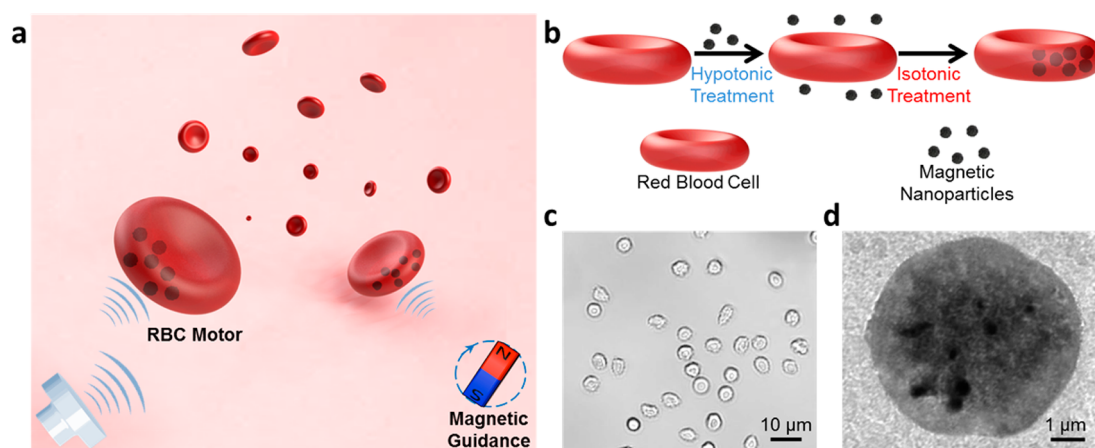
©2014 American Chemical Society

Figure 1. Red blood cell (RBC) motors. (a) Schematic illustration of magnetically guided, ultrasound-propelled RBC micromotors in whole blood. (b) Preparation of the RBC motors: magnetic nanoparticles are loaded into regular RBCs by using a hypotonic dilution encapsulation method. (c) Optical and (d) transmission electron microscopy images of the RBC motors.

Here we demonstrate the attractive behavior of an ultrasound-powered, magnetically switchable RBC-based micromotor (denoted RBC motor). Recent efforts have demonstrated that the ultrasound field can trigger the propulsion of microscale objects, and that such movement is driven by the interaction between the objects and the distribution of acoustic forces within the field.[33,34] The new RBC motors are prepared by loading iron oxide nanoparticles into RBCs. The propulsion of the RBC motor can be attributed to the asymmetric distribution of iron oxide nanoparticles within the cell, which is critical for ultrasound-powered motion.[35] The RBC motor is propelled by the pressure gradient generated by the ultrasound waves due to the inherent asymmetric geometry of the RBC as well as the asymmetric distribution of magnetic particles inside the RBCs. The latter also provides a net magnetization that enables magnetic alignment and guidance under acoustic propulsion. The magnetic guidance (orientation) of these RBC motors can be switched "on" and "off" by applying an external magnetic field. The resulting RBC motors possess highly efficient, ultrasound-powered, magnetically guided propulsion (Figure 1a). Of particular interest is the efficient prolonged movement that the RBC motors display in the bloodstream over an extended period of time with no apparent biofouling effects. The RBC membrane serves as an intrinsic shield to protect the magnetic nanoparticles (MNPs) from etching by coexisting ions (*e.g.*, chlorides, phosphates) in the blood, hence obviating the need for commonly used protective coating.[36] Moreover, one of the most important factors of micromotors for biomedical applications is biocompatibility or the ability of the motors to prevent detection and uptake by immune cells such as macrophages. Due to their inherent biomimetic properties, the new RBC motors are not susceptible to uptake by macrophages, displaying remarkable biocompatibility essential for practical biomedical uses.

RESULTS AND DISCUSSION

The new RBC motors were prepared using a hypotonic dilution/encapsulation method to load iron oxide nanoparticles (20 nm) into RBCs (Figure 1b).[37] In the experiment, the RBCs were briefly incubated with citrate-stabilized iron oxide nanoparticles in hypo-osmotic lysing buffer to undergo a hypotonic hemolysis process at low temperature (4 °C). It has been reported that the influx of fluid creates pores with a diameter of up to 100 nm in the RBC membrane.[38] These nanopores allow for inward diffusion of the magnetic nanoparticles from the surrounding medium into the cell and in parallel allow for outward diffusion of intracellular hemoglobin protein. The cells were held at low temperature for 1 h so that the inner and outer particle concentrations reach equilibrium. Upon equilibrium, the solution reached isotonicity when the cell membrane was resealed by restoration of osmolarity. The temperature was then increased to 37 °C, and the encapsulated magnetic nanoparticles were trapped inside the RBCs. Such loading protocol resulted in efficient encapsulation of magnetic nanoparticles into cells while minimizing damage to the cell membrane. The optical microscope image in Figure 1c demonstrates that the RBC motors mostly retain the characteristic erythrocyte shape with a diameter of 6−8 μm. The transmission electron microscopy (TEM) image in Figure 1d shows the magnetic nanoparticles as black spots within the RBC, located primarily inside the cell. During the hypotonic process, the nanoparticles aggregate asymmetrically within the RBCs into large magnetic particles,[39−41] which reflects the interaction between the nanoparticles and the remaining hemoglobin proteins to form an agglomerate. Such asymmetric distribution of the magnetic nanoparticle aggregates provides a net magnetization to the cellular structure that subsequently allows magnetic alignment under an external magnetic field.

The RBC motors are acoustically powered and magnetically guided by an applied, external magnetic field.
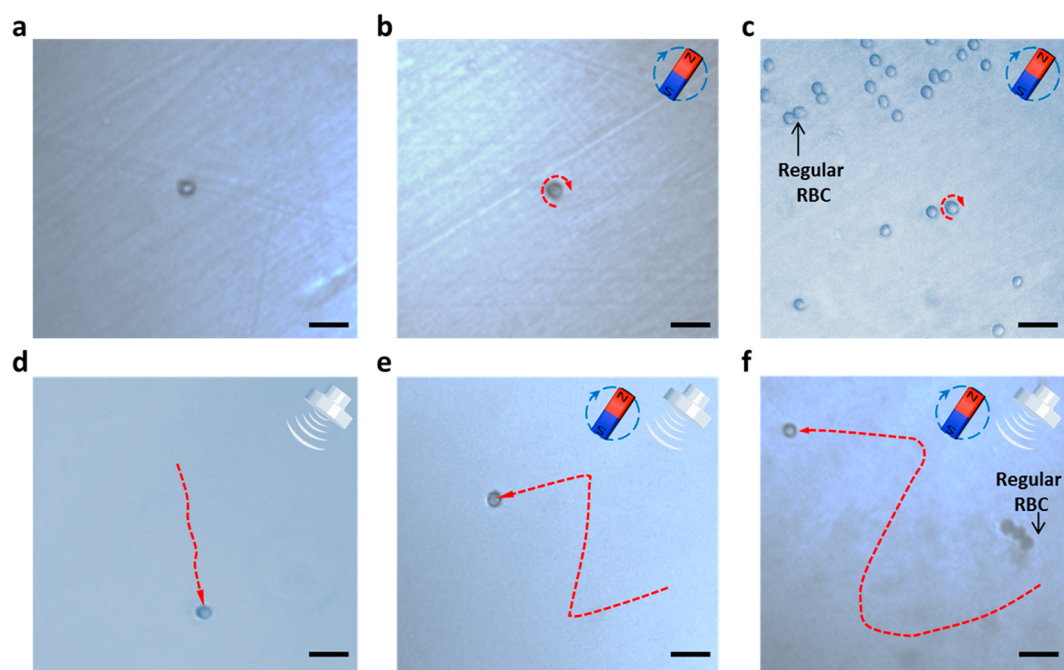
Figure 2. Propulsion performance of RBC motors. The RBC motor, suspended in PBS solution, was subjected to various external stimulus conditions, including (a) without any stimulus, (b) under magnetic field alone, (c) under magnetic field in the presence of regular (nonmagnetic) RBCs, (d) under ultrasound field alone, (e) under both magnetic and ultrasound fields, and (f) under both magnetic and ultrasound fields in the presence of regular RBCs (nonmagnetic). Scale bars, 20 μm. Corresponding videos are provided in the Supporting Information (video S1).

In order to prove that the RBC motors hold efficient guided motion under the combination of ultrasound and magnetic fields, a set of control experiments was conducted under different combinations of these external stimuli. Figure 2a and corresponding supplementary movie S1 show that the position of the RBC motor remained stationary in the absence of both ultrasound and magnetic fields. Application of a rotating magnetic field to the RBC motor, in the absence of ultrasound field, resulted in corresponding rotation of the motor, yet without its displacement (Figure 2b and video S1), reflecting that the magnetic field affects only the orientation of the magnetic nanoparticles inside the RBC motor. Such magnetically driven rotation was not observed for regular RBCs that do not contain internal magnetic nanoparticles (Figure 2c and video S1). Application of an ultrasound field alone to the RBC motor led to directional motion of the motor, as displayed by the tracking line in Figure 2d and video S1. It has been well-documented that blood cells and micro-organisms migrate toward pressure nodes under the ultrasound field.[33] However, such responses of regular cells are different from the controlled propulsion of MNP-loaded RBC motors. As illustrated in Figure 2e and video S1, the simultaneous application of both the ultrasound and magnetic fields results in a guided motion of the RBC motor, reflecting the reversible alignment of the magnetization vector (discussed below). In order to confirm that this guided motion is selective to the RBC motors and not to other coexisting micro-objects, additional control experiments were performed by using regular RBCs (nonmagnetic) as a negative control. Figure 2f and corresponding supplementary video S1 illustrate that, when both ultrasound and magnetic fields were applied to the system containing the regular and magnetic RBCs, only the RBC motors exhibited controlled motion (with a "Z" shape trajectory).

The magneto-switchable guidance of the RBC motor is demonstrated in Figure 3. Application of the magnetic field (while the ultrasound power is on) provides a net magnetization that enables magnetic alignment and reversible guidance under the acoustic propulsion (Figure 3a). The time-lapse image in Figure 3b,c illustrates such reversible, magneto-switchable, controlled acoustic propulsion. The on/off magnetic switching allowed the motion of the RBC motor to be periodically reoriented (Figure 3b,c). Compared with the controlled movement of the RBC motor (Figure 3b), the natural RBC exhibited no significant change in direction upon turning the magnetic field on or off (Figure 3c). The switchable behavior of the RBC motor observed in Figure 3 demonstrates the crucial role of the magnetic nanoparticles in controlling the direction of the ultrasound-powered RBC motor. We hypothesize that the ultrasound propulsion of the RBC motor is caused by an asymmetric distribution of the encapsulated magnetic nanoparticles inside the RBC motor (that leads to asymmetric intracellular density gradient) as well as the inherent asymmetric geometry of the RBC. Further, the asymmetry of the magnetic particles within the RBC creates a net magnetization within the cell in the
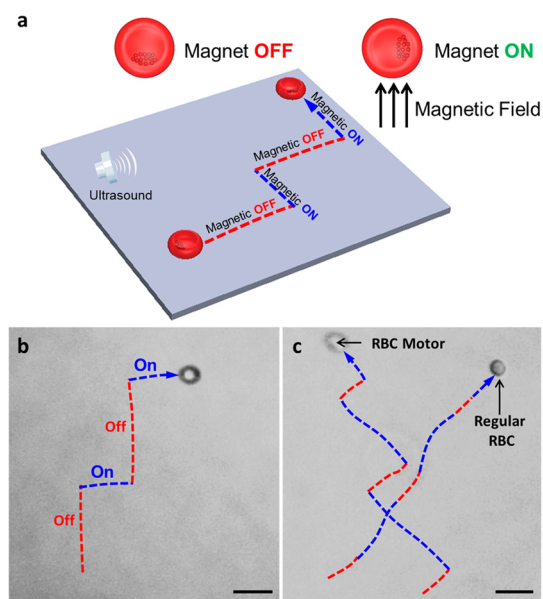
Figure 3. Magneto-switchable guidance of ultrasound-powered RBC motor. (a) Schematic illustration showing the projected motion trajectory of the RBC motor under ultrasound field with on−off switchable magnetic field. (b) Actual time-lapse image, from corresponding video S2, illustrating the movement of the RBC motor under ultrasound field upon turning the magnetic field on and off; (c) same as in (b) but in the presence of a regular natural RBC as a control. Scale bars, 20 μm.

presence of the magnetic field. The latter aligns the magnetization vector to become parallel with the field, altering the direction of the asymmetry. The magnetic orientation of the RBC motors can thus be switched on and off by applying an external magnetic field. These data clearly indicate that encapsulating magnetic nanoparticles into the RBC motors, along with application of magnetic field, is essential for creating guided motion under the ultrasound field.

For practical biomedical applications, it is critical to test the propulsion performance of the RBC motor in relevant biological environments.[42] As illustrated in Figure 4a and corresponding video S3, the RBC motors can operate readily in diverse media ranging from PBS buffer solution to undiluted whole blood. The ultrasound-powered RBC motors display a linear movement under the magnetic alignment. The 3 s track lines of such movement (Figure 4a) indicate that the speed of the RBC motor decreased from 16 μm/s in the PBS solution to 13, 12, and 5 μm/s in the cell medium, serum, and whole blood, respectively, reflecting the increased environmental viscosity of these biofluids. The average speeds of the RBC motor in different biological media are measured and displayed in Figure 4b. While these media affect the motor speed, the RBC motor still moves efficiently in the different environments, indicating the robustness of the motor for diverse biomedical applications.

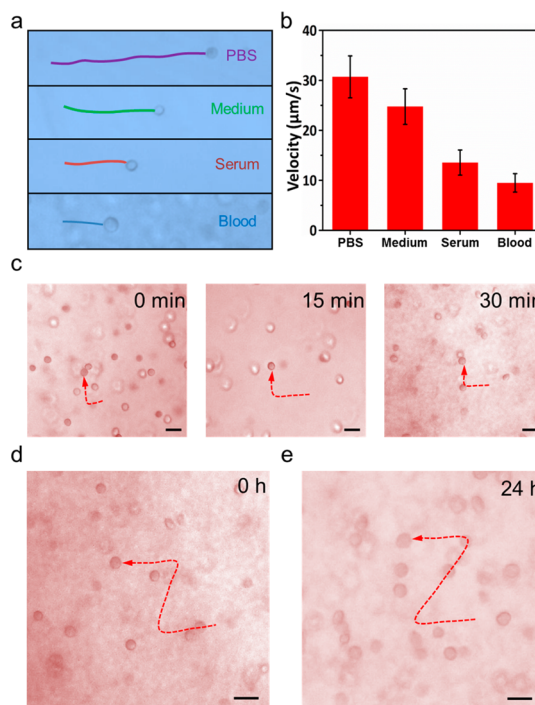Of particular biomedical significance is the efficient propulsion and behavior of the RBC motor in undiluted

Figure 4. Movement of RBC motors in various media. (a) Images illustrating the propulsion of the RBC motor in PBS, cell culture medium, serum, and whole blood, taken from corresponding video S3. (b) Quantitative velocity of the RBC motor in different media at ultrasound voltage of 3 V and a frequency of 2.93 MHz. (c) Swimming behavior of the RBC motor in undiluted whole blood over 30 min, taken from corresponding video S4. Scale bars, 10 μm. (d,e) Images showing the propulsion of the RBC motor in whole blood before (d) and after (e) a 24 h incubation in the whole blood. Scale bars, 10 μm.

whole blood. Most of the previous micromotor studies in biological fluids were focused on serum or highly diluted blood samples. Ghosh reported recently the magnetically actuated movement of cytocompatible ferrite-coated helical nanohelices in whole blood.[36] The RBC motor displayed magnetically guided movement in undiluted whole blood over both short and long periods, consistent with the long life span of natural RBCs.[43] For example, the time-lapse images in Figure 4c and corresponding video S4 illustrate controlled movement of RBC motors through whole blood at 15 min intervals over a 30 min period. During this prolonged operation, the motor displayed not only controllable movement with orthogonal turning but also a negligible change of speed (14 μm/s at 0 min, 13 μm/s at 15 min, and 14 μm/s at 30 min). Figure 4d illustrates such propulsion of the RBC motor in whole blood along a predetermined Z-shaped trajectory. To demonstrate their resistance to biofouling, the RBC motor was incubated in undiluted whole blood for 24 h followed by testing its performance. As shown in Figure 4d,e and video S5, the motor exhibits a similar magnetically guided acoustic propulsion before and after the incubation; the "Z" trajectory of the RBC motor and the migration of regular RBCs with a speed of
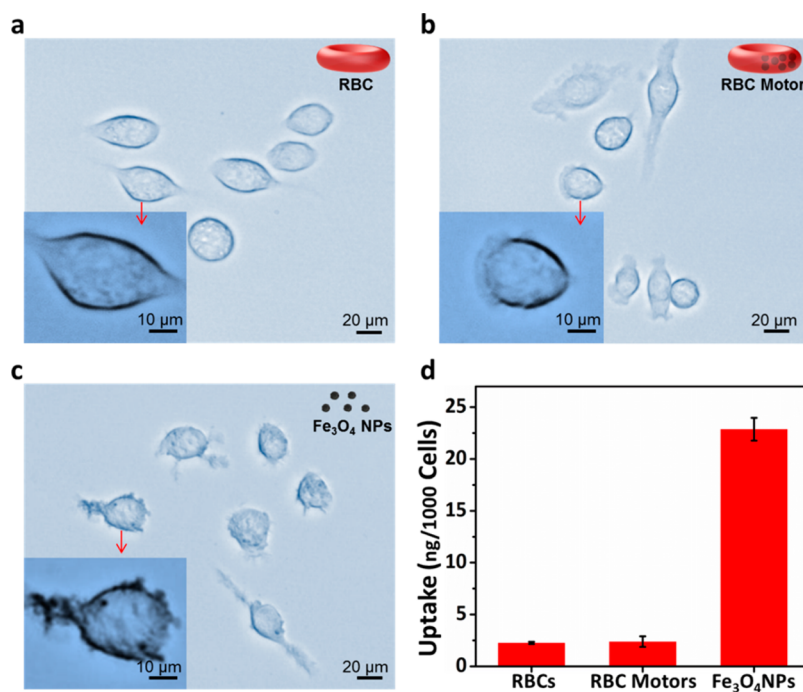
Figure 5. Macrophage uptake study to illustrate the biocompatibility of RBC motors. (a–c) Bright-field microscopic images of J774 murine macrophage cells incubated for 30 min, with regular RBCs, RBC motors, and iron oxide nanoparticles (Fe$_3$O$_4$ NPs, with equal amounts of iron to that of the RBC motors), respectively. (d) Quantitative analysis of macrophage uptake of RBC motors and iron oxide NPs determined by ICP-MS measurements.

5 μm/s can be observed. Note that such long immersion in whole blood has a minimal effect upon the speed of the RBC motor (12 *vs* 11 μm/s, before *vs* after the incubation), reflecting the absence of protein biofouling and salt-etching effects on the motor behavior. Overall, the data of Figure 4 clearly indicate that the RBC motor can operate in diverse environments, confirming the protection of the magnetic nanoparticles by the RBC membrane.

An important feature of the RBC motor is its anti-phagocytosis capability against macrophages, which is crucial for evading the immune attack for prolonged lifetime in the bloodstream. The RBC motor retains intact membrane structure and antigens of natural RBCs including CD47 that prevents phagocytosis by macrophages through its interaction with inhibitory receptor SIRPα.[44,45] Therefore, the RBC motor is expected to share the functionality of natural RBCs. To investigate the biocompatibility of the RBC motor, a macrophage uptake study was carried out by cultivating the J774 murine macrophage cells with RBC motors or unencapsulated magnetic nanoparticles for 1 h. To establish samples with equal amounts of iron, the magnetic nanoparticles were obtained from the same amount of RBC motors which are completely lysed by the addition of Triton X-100. The macrophages with natural RBCs were cultivated as a background control, which showed negligible uptake of RBCs (Figure 5a). Similar to natural RBCs, the RBC motors showed inhibited macrophage uptake, as well (Figure 5b). In contrast, the incubation of macrophages with unencapsulated magnetic nanoparticles resulted in a significant number of dark spots in the intracellular and perinuclear regions of the cells, indicating that the magnetic nanoparticles were actively taken up by the cells (Figure 5c). Inductively coupled plasma/mass spectrometry (ICP-MS) analysis was conducted to further quantify the iron uptake by the macrophage cells. As shown in Figure 5d, an uptake of 22.88 ng iron per 1000 cells was observed from the magnetic nanoparticles, while the RBC motors had an uptake of 2.38 ng per 1000 macrophage cells. The near 10-fold reduction in the amount of iron clearly demonstrates that the RBC motor can effectively inhibit the uptake by the macrophage cells. The inhibition is largely due to the immunosuppressive antigens of the RBC membrane present on the RBC motors; the encapsulation of magnetic particles exhibits a negligible effect on the stealthy properties of the RBC.

To test the tolerability of regular RBCs to the long period of ultrasound treatment, we next examined the properties of natural RBCs propelled by ultrasound at different transducer voltages (1–6 V) for a period of 1 h. The images of Figure 6a,b show a 1% suspension of regular RBCs before and after the ultrasound treatment, respectively. The geometry of RBCs exhibited negligible change after the treatment, indicating that the ultrasound field did not cause adverse effect on the RBCs. Moreover, the absorption spectrum of regular RBCs, over the 300–800 nm wavelength range, showed no detectable change at various ultrasound powers (Figure 6c). The ultrasound-treated regular
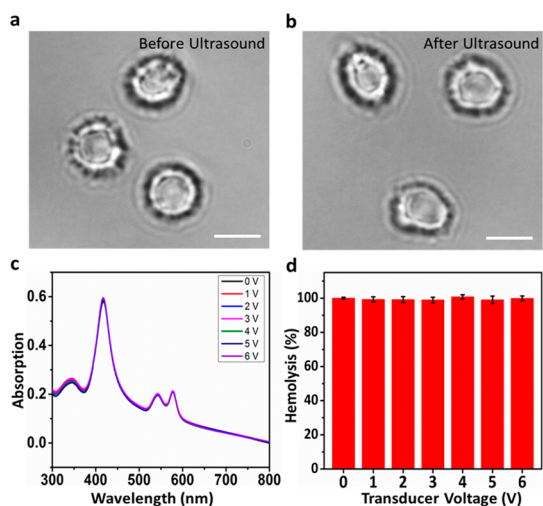
Figure 6. Tolerability of regular RBCs under ultrasound operations. (a,b) Optical images of regular RBCs before and after the ultrasonic treatment, respectively. Scale bars, 5 μm. (c) Absorption spectra of regular RBCs under ultrasound field with an applied frequency of 2.93 MHz and at different transducer voltages (0−6 V). (d) Relative hemolysis of regular RBCs under various ultrasound transducer voltages.

RBCs were next subjected to hemolytic lysis to quantify the remaining hemoglobin within these cells by measuring the hemoglobin absorbance at 540 nm. We found that all hemoglobin was retained inside the cells after the ultrasound treatment, corresponding to near 100% hemolysis after the hemolytic treatment (Figure 6d). Such negligible change in the degree of hemolysis further confirms the stability of regular RBCs under the ultrasound field.

CONCLUSIONS

We reported an RBC-derived approach for developing a new generation of cell-based micromotor that is powered by ultrasound and activated by a magnetic field. The RBC motor was fabricated by loading magnetic nanoparticles into natural RBCs. Switchable guided propulsion of RBC motors can be achieved by using a combination of the ultrasound and magnetic fields. The RBC motors can perform controlled propulsion in undiluted whole blood over extended periods with no apparent biofouling. The inhibited macrophage uptake confirms the biocompatibility of the RBC motors. The ability to load natural RBCs with a variety of functional components,[46] together with the efficient propulsion in a broad spectrum of biological fluids, holds great promise for developing multifunctional cell-based micromotors for a variety of *in vitro* and *in vivo* biomedical applications and for bridging the gap between synthetic motors and the biological world.

EXPERIMENTAL SECTION

Synthesis of Citrate-Stabilized Magnetic Nanoparticles. Citrate-stabilized Fe_3O_4 nanoparticles were synthesized using the previously reported protocol.[47] Briefly, a mixture of 0.43 g of $FeCl_2$ and 0.70 g of $FeCl_3$ was mixed in 40 mL of water, which was degassed with nitrogen before mixing under the protection of nitrogen. Subsequently, 2 mL of NH_4OH was added to the mixture solution under vigorous stirring and heated at 80 °C for an additional 30 min. The supernatant was discarded while the nanoparticles were obtained in the reaction flask using a magnet, and then fresh degassed water was added. Citric acid solution (2 mL, 0.5 g/mL) was added, and the reaction mixture was maintained at 95 °C for 90 min. The reaction mixture was allowed to cool to room temperature under nitrogen. The nanoparticle suspension was washed three times with deionized water and then collected for the subsequent use.

Encapsulation of Magnetic Particles in RBCs. Fresh RBCs were collected from six-week-old male ICR mice and anticoagulated with ethylenediamine tetraacetate. The cells were rinsed three times with PBS (300 mOsm, pH 8). For encapsulating magnetic nanoparticles into the RBCs, 300 μL suspension of RBC and 300 μL suspension of citrate-stabilized iron oxide nanoparticles were mixed, which led to a hypotonic condition (final osmotic pressure in RBC suspension, 100−160 mOsm). The RBCs were incubated under stirring at 4 °C for 1 h. The loaded RBCs were washed three times with PBS (300 mOsm, pH = 8) at room temperature to remove the free hemoglobin and excess Fe_3O_4 nanoparticles. The resulting RBCs were resealed by incubation in 100 mL of PBS at 37 °C for 1 h.

Ultrasound Equipment. The ultrasound experiments were carried out in a cell, as was reported previously.[48,49] The cell was made in a covered glass slide (75 × 25 × 1 mm). A piezoelectric transducer (PZT), consisting of a 0.5 mm thick ring with a 10 mm outside diameter and 5 mm inner diameter, was attached to the bottom center of the glass slide to create the ultrasonic field. The continuous ultrasound sine wave was applied through the PZT, *via* an Agilent 15 MHz arbitrary waveform generator, which was connected to a power amplifier. The continuous sine waveform had a frequency of 2.93 MHz and a voltage amplitude varied between 0 and 10.0 V, as needed for controlling the intensity of the ultrasonic wave. The electric signal was monitored using a 20 MHz Tektronix 434 storage oscilloscope.

Conflict of Interest: The authors declare no competing financial interest.

Supporting Information Available: Videos of the propulsion of the RBC motors. This material is available free of charge *via* the Internet at http://pubs.acs.org.

REFERENCES AND NOTES

1. Dreyfus, R.; Baudry, J.; Roper, M. L.; Fermigier, M.; Stone, H. A.; Bibette, J. Microscopic Artificial Swimmers. *Nature* **2005**, *437*, 862–865.
2. Paxton, W. F.; Kistler, K. C.; Olmeda, C. C.; Sen, A.; St. Angelo, S. K.; Cao, Y.; Mallouk, T. E.; Lammert, P. E.; Crespi, V. H. Catalytic Nanomotors: Autonomous Movement of Striped Nanorods. *J. Am. Chem. Soc.* **2004**, *126*, 13424–13431.
3. Wilson, D. A.; Nolte, R. J. M.; van Hest, J. C. M. Autonomous Movement of Platinum-Loaded Stomatocytes. *Nat. Chem.* **2012**, *4*, 268–274.
4. Weiss, P. S. Nanotechnology: A Molecular Four-Wheel Drive. *Nature* **2011**, *479*, 187–188.
5. Wang, J. *Nanomachines: Fundamentals and Applications*; Wiley-VCH: Weinheim, Germany, 2013.

6. Mei, Y. F.; Solovev, A. A.; Sanchez, S.; Schmidt, O. G. Rolled-up Nanotech on Polymers: From Basic Perception to Self-Propelled Catalytic Microengines. *Chem. Soc. Rev.* **2011**, *40*, 2109–2119.

7. Loget, G.; Kuhn, A. Electric Field-induced Chemical Locomotion of Conducting Objects. *Nat. Commun.* **2011**, *2*, 535.

8. van Rhee, P. G.; Rikken, R. S. M.; Abdelmohsen, L. K. E. A.; Maan, J. C.; Nolte, R. J. M.; van Hest, J. C. M.; Christianen, P. C. M.; Wilson, D. A. Polymersome Magneto-Valves for Reversible Capture and Release of Nanoparticles. *Nat. Commun.* **2014**, *5*, 5010.

9. Li, J.; Gao, W.; Dong, R.; Pei, A.; Sattayasamitsathit, S.; Wang, J. Nanomotor Lithography. *Nat. Commun.* **2014**, *5*, 5026.

10. Wu, J.; Balasubramanian, S.; Kagan, D.; Manesh, K. M.; Campuzano, S.; Wang, J. Motion-Based DNA Detection Using Catalytic Nanomotors. *Nat. Commun.* **2010**, *1*, 36.

11. Sengupta, S.; Patra, D.; Ortiz-Rivera, I.; Agrawal, A.; Shklyaev, S.; Dey, K. K.; Córdova-Figueroa, U.; Mallouk, T. E.; Sen, A. Self-Powered Enzyme Micropumps. *Nat. Chem.* **2014**, *6*, 415–422.

12. Ikezoe, Y.; Washino, G.; Uemura, T.; Kitagawa, S.; Matsui, H. Autonomous Motors of a Metal-Organic Framework Powered by Reorganization of Self-Assembled Peptides at Interfaces. *Nat. Mater.* **2012**, *11*, 1081–1085.

13. Solovev, A. A.; Sanchez, S.; Pumera, M.; Mei, Y. F.; Schmidt, O. G. Magnetic Control of Tubular Catalytic Microbots for the Transport, Assembly, and Delivery of Micro-objects. *Adv. Funct. Mater.* **2010**, *20*, 2430–2435.

14. Guix, M.; Mayorga-Martinez, C. C.; Merkoçi, A. Nano/Micromotors in (Bio)Chemical Science Applications. *Chem. Rev.* **2014**, *114*, 6285–6322.

15. Ismagilov, R. F.; Schwartz, A.; Bowden, N.; Whitesides, G. M. Autonomous Movement and Self-Assembly. *Angew. Chem., Int. Ed.* **2002**, *114*, 652–654.

16. Wang, W.; Duan, W.; Ahmed, S.; Mallouk, T. E.; Sen, A. Small Power: Autonomous Nano- and Micromotors Propelled by Self-Generated Gradients. *Nano Today* **2013**, *8*, 531–554.

17. Tottori, S.; Zhang, L.; Peyer, K. E.; Nelson, B. J. Assembly, Disassembly, and Anomalous Propulsion of Microscopic Helices. *Nano Lett.* **2013**, *13*, 4263–4268.

18. Wang, W.; Castro, L. A.; Hoyos, M.; Mallouk, T. E. Autonomous Motion of Metallic Microrods Propelled by Ultrasound. *ACS Nano* **2012**, *6*, 6122–6132.

19. Fischer, P.; Ghosh, A. Magnetically Actuated Propulsion at Low Reynolds Numbers: Towards Nanoscale Control. *Nanoscale* **2011**, *3*, 557–563.

20. Schamel, D.; Mark, A. G.; Gibbs, J. G.; Miksch, C.; Morozov, K. I.; Leshansky, A. M.; Fischer, P. Nanopropellers and Their Actuation in Complex Viscoelastic Media. *ACS Nano* **2014**, *8*, 8794–8801.

21. Zhang, L.; Hong, L.; Yu, Y.; Bae, S. C.; Granick, S. Nanoparticle-Assisted Surface Immobilization of Phospholipid Liposomes. *J. Am. Chem. Soc.* **2006**, *128*, 9026–9027.

22. Zhang, L.; Spurlin, T. A.; Gewirth, A. A.; Granick, S. Electrostatic Stitching in Gel-Phase Supported Phospholipid Bilayers. *J. Phys. Chem. B* **2005**, *110*, 33–35.

23. Love, K. T.; Mahon, K. P.; Levins, C. G.; Whitehead, K. A.; Querbes, W.; Dorkin, J. R.; Qin, J.; Cantley, W.; Qin, L. L.; Racie, T.; *et al.* Lipid-like Materials for Low-Dose, *In Vivo* Gene Silencing. *Proc. Natl. Acad. Sci. U.S.A.* **2010**, *107*, 1864–1869.

24. Celiz, A. D.; Smith, J. G. W.; Langer, R.; Anderson, D. G.; Winkler, D. A.; Barrett, D. A.; Davies, M. C.; Young, L. E.; Denning, C.; Alexander, M. R. Materials for Stem Cell Factories of the Future. *Nat. Mater.* **2014**, *13*, 570–579.

25. Yang, F.; Cho, S. W.; Son, S. M.; Bogatyrev, S. R.; Singh, D.; Green, J. J.; Mei, Y.; Park, S.; Bhang, S. H.; Kim, B. S.; *et al.* Genetic Engineering of Human Stem Cells for Enhanced Angiogenesis Using Biodegradable Polymeric Nanoparticles. *Proc. Natl. Acad. Sci. U.S.A.* **2010**, *107*, 3317–3322.

26. Hu, C. M.; Fang, R. H.; Luk, B. T.; Zhang, L. Nanoparticle-Detained Toxins for Safe and Effective Vaccination. *Nat. Nanotechnol.* **2013**, *8*, 933–938.

27. Zhang, K.; Zhang, L.; Weinreb, R. N. Ophthalmic Drug Discovery: Novel Targets and Mechanisms for Retinal Diseases and Glaucoma. *Nat. Rev. Drug Discovery* **2012**, *11*, 541–559.

28. Pierigè, F.; Serafini, S.; Rossi, L.; Magnani, M. Cell-Based Drug Delivery. *Adv. Drug Delivery Rev.* **2008**, *60*, 286–295.

29. Brähler, M.; Georgieva, R.; Buske, N.; Müller, A.; Müller, S.; Pinkernelle, J.; Teichgräber, U.; Voigt, A.; Bäumler, H. Magnetite-Loaded Carrier Erythrocytes as Contrast Agents for Magnetic Resonance Imaging. *Nano Lett.* **2006**, *6*, 2505–2509.

30. Lee, J.; Choi, J.; Park, J. H.; Kim, M. H.; Hong, D.; Cho, H.; Yang, S. H.; Choi, I. S. Cytoprotective Silica Coating of Individual Mammalian Cells through Bioinspired Silicification. *Angew. Chem., Int. Ed.* **2014**, *53*, 8056–8059.

31. Muzykantov, V. R. Drug Delivery by Red Blood Cells: Vascular Carriers Designed by Mother Nature. *Expert Opin. Drug Delivery* **2010**, *7*, 403–427.

32. Yoo, J. W.; Irvine, D. J.; Discher, D. E.; Mitragotri, S. Bio-Inspired, Bioengineered and Biomimetic Drug Delivery Carriers. *Nat. Rev. Drug Discovery* **2011**, *10*, 521–535.

33. Ding, X.; Lin, S.-C. S.; Kiraly, B.; Yue, H.; Li, S.; Chiang, I. K.; Shi, J.; Benkovic, S. J.; Huang, T. J. On-Chip Manipulation of Single Microparticles, Cells, and Organisms Using Surface Acoustic Waves. *Proc. Natl. Acad. Sci. U.S.A.* **2012**, *109*, 11105–11109.

34. Wang, W.; Li, S.; Mair, L.; Ahmed, S.; Huang, T. J.; Mallouk, T. E. Acoustic Propulsion of Nanorod Motors Inside Living Cells. *Angew. Chem., Int. Ed* **2014**, *126*, 3265–3268.

35. Nadal, F.; Lauga, E. Asymmetric Steady Streaming as a Mechanism for Acoustic Propulsion of Rigid Bodies. *Phys. Fluids* **2014**, *26*, 082001.

36. Venugopalan, P. L.; Sai, R.; Chandorkar, Y.; Basu, B.; Shivashankar, S.; Ghosh, A. Conformal Cytocompatible Ferrite Coatings Facilitate the Realization of a Nanovoyager in Human Blood. *Nano Lett.* **2014**, *14*, 1968–1975.

37. Kolesnikova, T. A.; Skirtach, A. G.; Möhwald, H. Red Blood Cells and Polyelectrolyte Multilayer Capsules: Natural Carriers *versus* Polymer-Based Drug Delivery Vehicles. *Expert Opin. Drug Delivery* **2013**, *10*, 47–58.

38. Delcea, M.; Sternberg, N.; Yashchenok, A. M.; Georgieva, R.; Bäumler, H.; Möhwald, H.; Skirtach, A. G. Nanoplasmonics for Dual-Molecule Release through Nanopores in the Membrane of Red Blood Cells. *ACS Nano* **2012**, *6*, 4169–4180.

39. Zhang, E.; Kircher, M. F.; Koch, M.; Eliasson, L.; Goldberg, S. N.; Renström, E. Dynamic Magnetic Fields Remote-Control Apoptosis *via* Nanoparticle Rotation. *ACS Nano* **2014**, *8*, 3192–3201.

40. Valberg, P. A.; Feldman, H. A. Magnetic Particle Motions within Living Cells. Measurement of Cytoplasmic Viscosity and Motile Activity. *Biophys. J.* **1987**, *52*, 551–561.

41. Wilhelm, C.; Billotey, C.; Roger, J.; Pons, J. N.; Bacri, J. C.; Gazeau, F. Intracellular Uptake of Anionic Superparamagnetic Nanoparticles as a Function of Their Surface Coating. *Biomaterials* **2003**, *24*, 1001–1011.

42. Gao, W.; Sattayasamitsathit, S.; Orozco, J.; Wang, J. Efficient Bubble Propulsion of Polymer-Based Microengines in Real-Life Environments. *Nanoscale* **2013**, *5*, 8909–8914.

43. Hu, C. M. J.; Zhang, L.; Aryal, S.; Cheung, C.; Fang, R. H.; Zhang, L. Erythrocyte Membrane-Camouflaged Polymeric Nanoparticles as a Biomimetic Delivery Platform. *Proc. Natl. Acad. Sci. U.S.A.* **2011**, *108*, 10980–10985.

44. Hu, C. M. J.; Fang, R. H.; Zhang, L. Erythrocyte-Inspired Delivery Systems. *Adv. Healthcare Mater.* **2012**, *1*, 537–547.

45. Fang, R. H.; Hu, C. M. J.; Zhang, L. Nanoparticles Disguised as Red Blood Cells To Evade the Immune System. *Expert Opin. Biol. Ther.* **2012**, *12*, 385–389.

46. Wang, C.; Sun, X.; Cheng, L.; Yin, S.; Yang, G.; Li, Y.; Liu, Z. Multifunctional Theranostic Red Blood Cells for Magnetic-Field-Enhanced *In Vivo* Combination Therapy of Cancer. *Adv. Mater.* **2014**, *26*, 4794–4802.

47. Lee, J.; Cohen, R. E.; Rubner, M. F. Heterostructured Magnetic Nanotubes. *Langmuir* **2006**, *23*, 123–129.

48. Xu, T.; Soto, F.; Gao, W.; Garcia-Gradilla, V.; Li, J.; Zhang, X.; Wang, J. Ultrasound-Modulated Bubble Propulsion of Chemically Powered Microengines. *J. Am. Chem. Soc.* **2014**, *136*, 8552–8555.

49. Garcia-Gradilla, V.; Orozco, J.; Sattayasamitsathit, S.; Soto, F.; Kuralay, F.; Pourazary, A.; Katzenberg, A.; Gao, W.; Shen, Y.; Wang, J. Functionalized Ultrasound-Propelled Magnetically Guided Nanomotors: Toward Practical Biomedical Applications. *ACS Nano* **2013**, *7*, 9232–9240.